ELSEVIER

Nuclear Instruments and Methods in Physics Research A 430 (1999) 423–434

NUCLEAR INSTRUMENTS & METHODS IN PHYSICS RESEARCH Section A

www.elsevier.nl/locate/nima

Measurement of cold neutron-beam focusing effect of a permanent sextupole magnet

Hirohiko M. Shimizu[a,*], Yoshiyuki Suda[b], Takayuki Oku[a], Haruko Nakagawa[b], Hiroshi Kato[a], Takashi Kamiyama[b], Chiko Otani[a], Hiromi Sato[a], Toshio Wakabayashi[c], Yoshiaki Kiyanagi[b]

[a]*The Institute of Physical and Chemical Research (RIKEN), 2-1 Hirosawa, Wako, Saitama 351-0198, Japan*
[b]*Graduate School of Engineering, Hokkaido University, Sapporo 060-8628, Japan*
[c]*Japan Nuclear Cycle Development Institute, 1-9-13 Akasaka, Minato, Tokyo 107-8445, Japan*

Received 1 February 1999

Abstract

The magnetic focus effect of cold neutron beam was measured using a permanent sextupole magnet and a gain of more than 35 was observed. The result was analyzed with a numerical simulation.

PACS: 03.75.B

Keywords: Cold neutron; Magnetic field gradient; Focus; Neutron lens; Neutron refractive optics; Sextupole

1. Introduction

Slow neutrons are widely used in the study of the structure and dynamics of materials. However, the applicable research field of neutron scattering experiment is limited by the low intensity of the neutron beam. Increasing the beam density enables us to extend the neutron scattering technique to smaller samples or apply it for spatial scanning of samples. Neutron focusing devices have been developed to localize and effectively increase the neutron beam intensity on the sample [1]. Most realized focusing devices comprise of reflective optical components. Neutron guide tubes are widely used in cold neutron experiments and a new device of multicapillary fiber is also used for experiments which require a high incident rate of neutrons such as for neutron-induced prompt gamma-ray analysis.

Simple focusing devices are not appropriate for other types of experiments which require a low beam divergence for a precise determination of scattering angle. The combination of reflective optics to suppress beam divergence reduces efficiency hence beam intensity. A possible solution is to employ refractive optics which enables the full use of neutron beam cross section. One method of neutron refractive optics is to apply an acceleration to the neutrons in an inhomogeneous magnetic field according to the interaction between neutron

* Corresponding author. Tel.: +81-48-462-1111 (ext.3481); fax: +81-48-467-9721.
E-mail address: shimizu@riken.go.jp (H.M. Shimizu)

0168-9002/99/$ - see front matter
PII: S0168-9002(99)00238-7

magnetic dipole moment and the external magnetic field [2–7]. The magnetic optics were studied as a velocity selector, polarizer, polarimeter, microscope etc. [3,8–11], and were applied to ultracold neutron storage ring for the measurement of neutron lifetime [12–15].

The focusing effects on a cold neutron beam were demonstrated using sextupole magnetic fields [16,17]. The magnetic neutron lens has the function of a concave lens together with that of a convex lens and can be used to decrease beam divergence. The focal condition of these neutron lenses are wavelength dependent. The strength of the magnetic lens can be adjusted electronically to match the incident neutron wavelengths if electromagnets are employed in the design. In addition, the neutron-spin polarization can be obtained since the magnetic lens functions as a convex lens and a concave lens depending on the neutron-spin polarity about the local magnetic field.

Alternative refractive optics using a compound lens was introduced and its focusing effect was demonstrated [18] with an acceptable level of attenuation of the neutron beam on transmission through the compound lens.

In this paper, we report recent results on the measurement of the focusing effect of a pulsed cold neutron beam with a permanent sextupole magnet. An analysis of the measured results with numerical simulations is also discussed.

2. Sextupole magnetic neutron lens

Neutron motion in a magnetic field is described by a coupled equation

$$\ddot{\boldsymbol{r}} = -\alpha\nabla(\boldsymbol{\sigma}\cdot\boldsymbol{B}) \tag{1}$$

$$\dot{\boldsymbol{\sigma}} = \gamma\boldsymbol{\sigma}\times\boldsymbol{B} \tag{2}$$

where $\boldsymbol{r}$ is neutron position, $\boldsymbol{\sigma}$ the unit vector parallel to neutron spin, $\alpha = |\mu/m| = 5.77\ \mathrm{m^2\,s^{-2}\,T^{-1}}$, $\gamma = 1.8\times10^8\ \mathrm{rad\ s^{-1}\,T^{-1}}$ the gyromagnetic ratio of neutron and $\boldsymbol{B}$ the external magnetic field. The dots above the variables represent the differentiation by the time t. Neutrons are accelerated along the gradient of the dipole coupling term and the neutron spin is rotated about the magnetic field direction at the angular frequency of $\omega_{\mathrm{L}} = \gamma B$.

Local magnetic fields at the neutron position vary as the neutrons travel in an inhomogeneous magnetic field. We define the angular velocity of magnetic field direction in the neutron rest frame as $\omega_{\mathrm{B}} = \dot{s}|\partial\hat{\boldsymbol{B}}/\partial s|$, where s is the coordinate taken on the neutron trajectory and $\hat{\boldsymbol{B}} = \boldsymbol{B}/|\boldsymbol{B}|$. If the local magnetic field is sufficiently strong, the neutron polarization along the magnetic field is adiabatically transported and is almost conserved. In this case, Eq. (1) can be simplified as

$$\ddot{\boldsymbol{r}} = \mp\alpha\nabla|\boldsymbol{B}| \tag{3}$$

where $\mp$ correspond to cases that neutron spins are parallel and antiparallel to the magnetic field, respectively.

We consider the case for unpolarized cold neutrons incident into a sextupole field which is defined as

$$\boldsymbol{B} = \frac{C}{2}\begin{pmatrix} y^2 - x^2 \\ 2xy \\ 0 \end{pmatrix} \tag{4}$$

where C is a positive constant. The z-axis is taken as parallel to the beam axis, and the x- and y-axes are perpendicular to the beam axis. Neutron spin is quantized along the local magnetic field on the entry to the magnetic field. Half the neutrons have their spin parallel to the local field and the other half antiparallel. For simplicity, we assume the adiabatic condition is always satisfied. The Eq. (3) becomes

$$\ddot{x} = \mp\omega^2 x, \qquad \ddot{y} = \mp\omega^2 y, \qquad \ddot{z} = 0 \tag{5}$$

where $\omega^2 = C\alpha$. The solution is given as

$$\begin{pmatrix} x & y \\ \xi & \eta \end{pmatrix} = M\begin{pmatrix} x_0 & y_0 \\ \xi_0 & \eta_0 \end{pmatrix}, \tag{6}$$

$$M = \begin{cases} M_{\mathrm{P}} = \begin{pmatrix} \cos\theta & \sin\theta \\ -\sin\theta & \cos\theta \end{pmatrix} & \text{parallel case} \\ M_{\mathrm{A}} = \begin{pmatrix} \cosh\theta & \sinh\theta \\ \sinh\theta & \cosh\theta \end{pmatrix} & \text{antiparallel case} \end{cases} \tag{7}$$

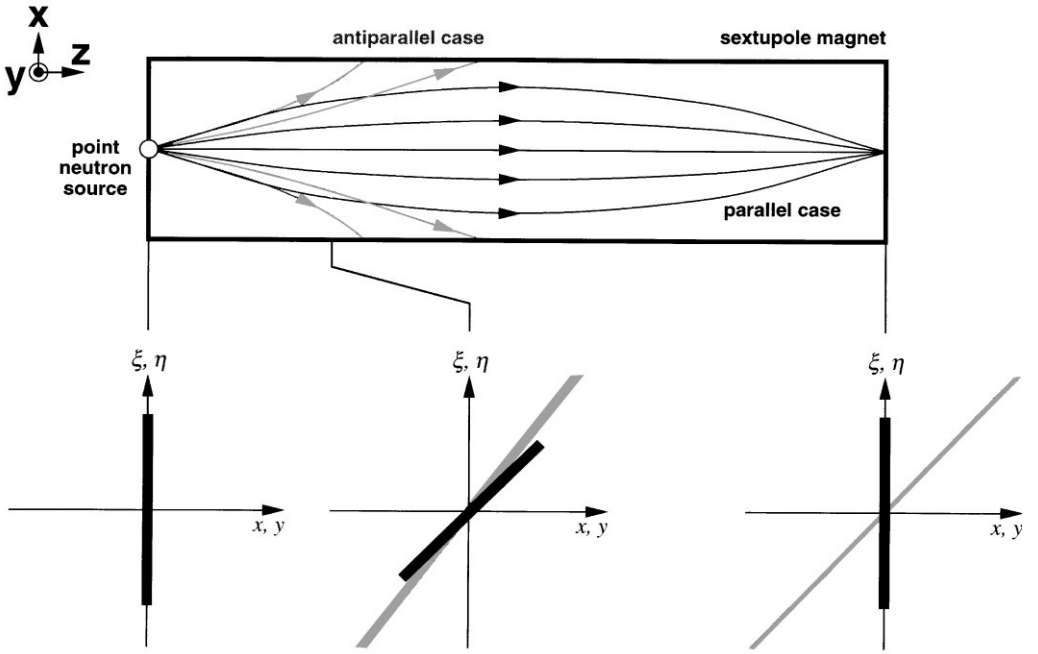

Fig. 1. Schematic illustration of trajectory and transformation on the $x\xi$-plane in a sextupole magnetic field for neutrons emitted from a point source located at the entrance of the magnetic field. Black and gray lines show trajectories of neutrons polarized parallel and antiparallel to the local magnetic field, respectively.

where $\xi = \dot{x}/\omega, \eta = \dot{y}/\omega$ and $\theta = \omega t$. ξ and η represent the beam divergences normalized by ω. Subscripts 0 indicate the value at $\theta = 0$. Matrix M_P rotates the neutron beam by $-\theta$ on the $x\xi$-plane and $y\eta$-plane, while M_A expands by e^{θ} along $(1,1)$ direction and compresses by $e^{-\theta}$ along $(-1,1)$ direction on the $x\xi$-plane and $y\eta$-plane. In the same way, the neutron motion out of the magnetic field is described by the matrix

$$M_0 = \begin{pmatrix} 1 & \theta \\ 0 & 1 \end{pmatrix}. \tag{8}$$

These transformation matrices do not change the area on the $x\xi$-plane and $y\eta$-plane consistent with the Liouville's theorem.

We consider the case of a point neutron source located at the entrance of a sextupole magnet as shown in Fig. 1. For simplicity, we discuss the beam transformation only on $x\xi$-plane. The beam is transformed in the same manner on $y\eta$-plane. The incident beam is represented as a given straight line on the ξ-axis. Half of the incident neutrons are rotated according to M_P and return to their original position on $x\xi$-plane after traveling $\theta = \pi$. The other half are transformed by M_A and swept away off the magnet axis. Therefore, the neutron density on axis at the magnet exit is enhanced at the focal condition $\theta = \pi$.

3. Experimental arrangement

The focusing effect of a sextupole magnet was studied by measuring the transmittance of cold neutrons through a sextupole magnet. The experimental setup is schematically shown in Fig. 2. A pulsed cold neutron beam from a liquid hydrogen moderator at the 45 MeV Electron Linear Accelerator Facility of Hokkaido University was incident to a 2 m long permanent sextupole magnet placed 2.75 m away from the moderator surface. We take the z-axis parallel to the beam direction, y-axis upward and x-axis perpendicular to both the z- and y-axes. We set $z = 0$ at the moderator surface.

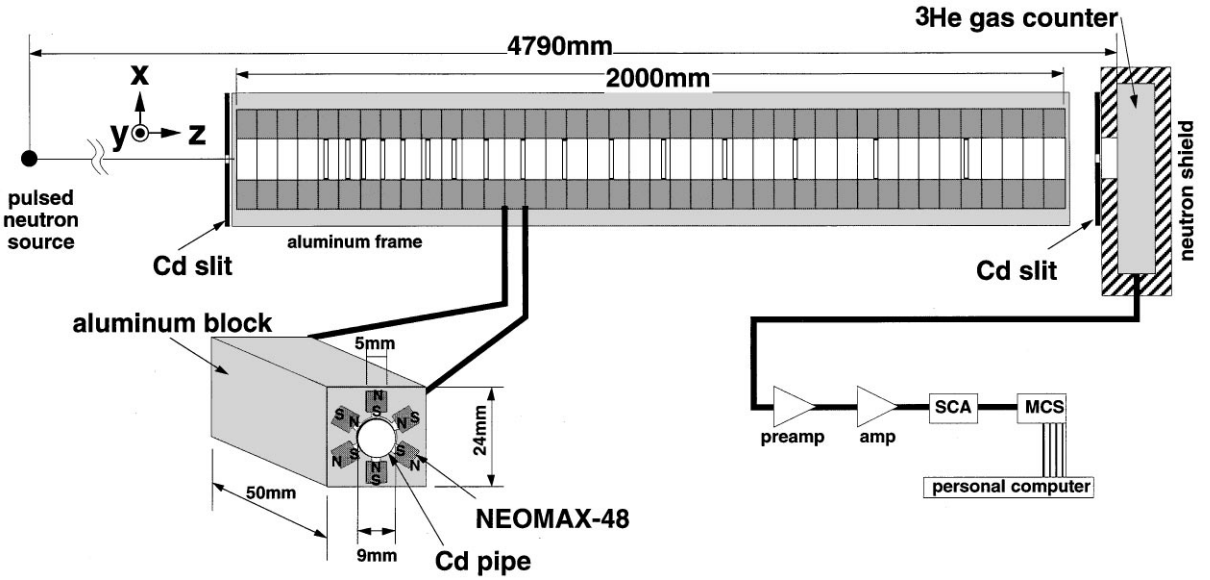

Fig. 2. Schematic view of experimental arrangement.

The primary electron beam was incident to a lead target with a repetition rate of 39 s^{-1}. The pulse width was 3 μs and the average current was 19.5 μA. The neutrons produced were moderated by a water premoderator and a liquid hydrogen moderator as shown in Fig. 3. The liquid hydrogen moderator was operated at 20 K. Moderated neutrons were incident to a 2000 mm long vacuum flight tube made of iron with an inner diameter of 230 mm. Both ends of the flight tube were 1 mm thick aluminum. The entrance and exit windows were located at $z \sim 700$ and 2700 mm, respectively.

The permanent sextupole magnet was placed downstream to the flight tube. 40 permanent sextupole units were assembled in an aluminum frame with an outer dimension of 48 mm × 48 mm × 2020 mm. The upstream surface of the aluminum frame was located at $z = 2750$ mm. Both ends of the aluminum frame was 10 mm thick and the sextupole magnetic field covered the region of $z = 2760$–4760 mm. Each sextupole unit was an aluminum block with the dimension of 24 mm × 24 mm × 50 mm. Six permanent magnet pieces of 5 mm × 5 mm × 50 mm NEOMAX48 [19] were inserted into holes within the aluminum block. The diameter of the center hole of the aluminum block was 10 mm. The strength of the sextupole field was measured to be $C = (3.5 \pm 0.6) \times 10^4$ T m^{-2}.

A cadmium slit with a circular hole of 2 mm diameter was attached at $z = 2750$ mm on the upstream surface of the aluminum frame. A ^{3}He gas counter was placed downstream of the magnet at $z = 4790$ mm. The counter was put in a neutron shielding case made of B_4C and mounted on a stage movable in the xy-plane. The aperture of the neutron shielding case was covered by another cadmium slit with a circular hole of 2 mm diameter. The cadmium slit was located at $z = 4780$ mm. Neutrons transmitted through both cadmium slits were detected by the counter and the signals were recorded by a multichannel scaler as a function of neutron time-of-flight (TOF). We denote the neutron count as a function of neutron wavelength as $N(\lambda)$.

Cadmium pipes were inserted in the aperture of the aluminum blocks for the suppression of neutron reflection on the inner surface of the magnet. The inner and outer diameters of the cadmium pipes were 9 and 10 mm, respectively. The inner surface of the aluminum hole was partially covered in the regions listed in Table 1. The covered regions

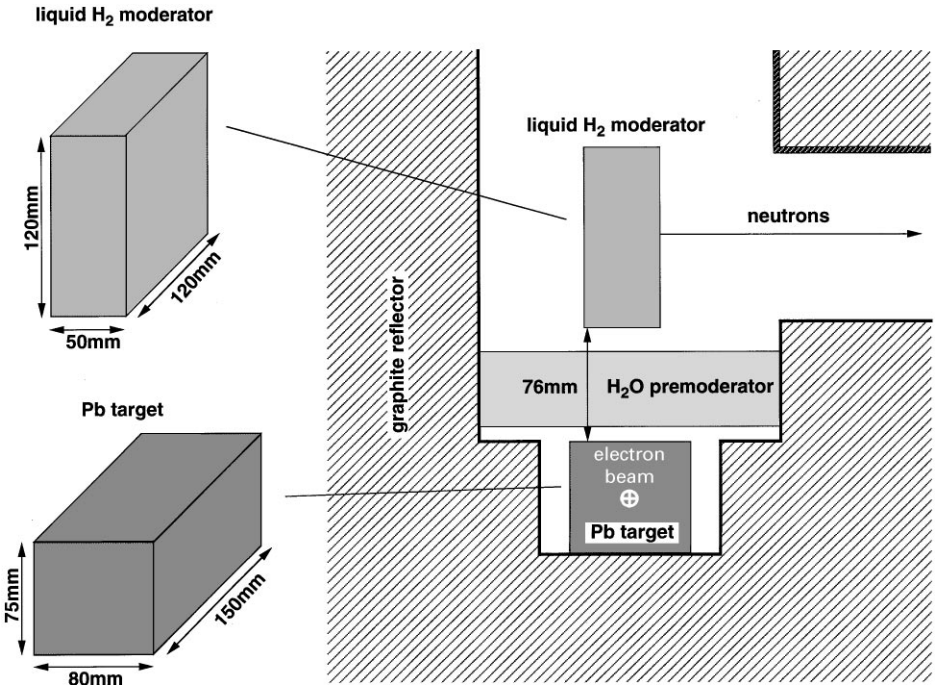

Fig. 3. Schematic view of the configuration of the neutron production target and the neutron moderator.

Table 1
z-coordinates of upstream and downstream ends of cadmium pipes installed inside the magnet aperture

	z (mm)	
No.	Upstream end	Downstream end
1	2949	2955
2	2977	2983
3	3010	3016
4	3047	3053
5	3090	3096
6	3138	3144
7	3193	3199
8	3257	3260
9	3329	3332
10	3412	3415
11	3527	3530
12	3615	3618
13	3738	3741
14	3879	3882
15	4041	4044
16	4225	4228
17	4436	4439
18	4676	4679

were selected so that the straight light coming from the aperture of the upstream cadmium does not directly hit the inner surface of magnet aperture. The partial coverage is sufficient according to the thickness of the cadmium pipes.

An identical configuration was prepared with non-magnetized NEOMAX48 pieces. We denote the neutron count obtained with the non-magnetized configuration as $N_0(\lambda)$. The effect of the magnetic field was measured as the deviation of the ratio $R(\lambda) = N(\lambda)/N_0(\lambda)$ from unity.

Fig. 4 shows the obtained TOF spectra of $N(\lambda)$ and $N_0(\lambda)$ when the detector is placed at $(x, y) = (0, 0)$ on the magnet axis. $N_{\text{in}}(\lambda)$ represents the neutron count obtained when all sextupole units were removed from the magnet frame, and three cadmium slits with circular holes of 5 mm diameter were placed inside the magnet frame with a spacing of 500 mm along the z-axis. The $N_{\text{in}}(\lambda)$ approximates the spectrum of incident neutron beam. Both $N(\lambda)$ and $N_0(\lambda)$ are increased at $\lambda \sim 3$ Å according to the neutron reflection on the inner

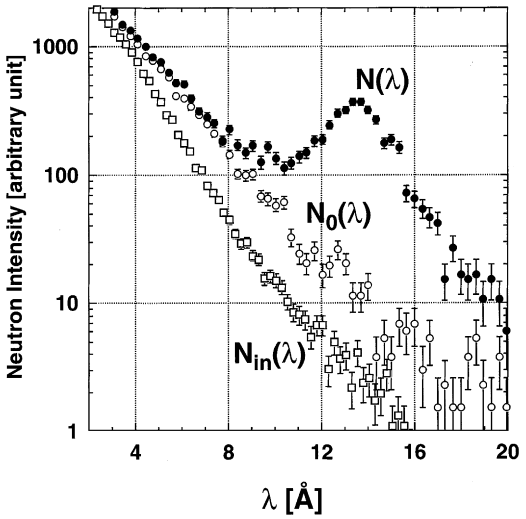

Fig. 4. Wavelength dependence of neutron intensity measured with the neutron detector located on the beam axis, e.g. at $(x, y) = (0, 0)$. Closed circles show the spectrum obtained with the sextupole magnet, open circles with the non-magnetized set and open squares without magnet units inside the magnet frame.

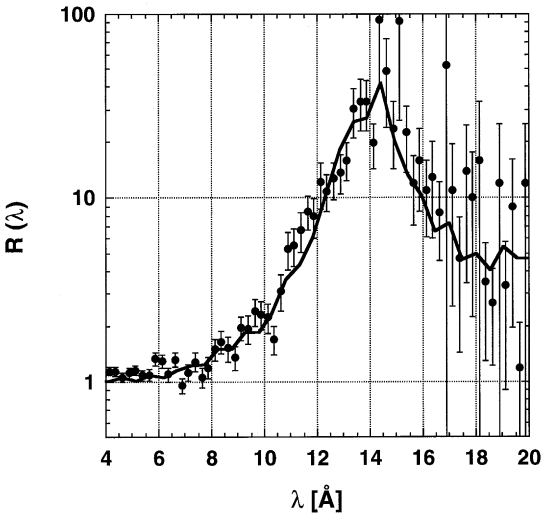

Fig. 5. Wavelength dependence of the magnet gain $R(\lambda)$ obtained on the magnet axis, e.g. at $(x, y) = (0, 0)$. The solid line shows the calculated value of $R(\lambda)$ with $\Gamma_e = 0.057$.

surface of the magnet aperture. The additional increase of $N(\lambda)$ was observed above $\lambda \sim 8$ Å, as a result of the focusing effect of the sextupole field. We define the gain of the magnet as the ratio $R(\lambda) = N(\lambda)/N_0(\lambda)$ since its deviation from unity unambiguously signals the magnetic focusing effect. The neutron density is increased also by the reflection on the inner surface of the magnet aperture. However, the reflected neutrons contaminate the output beam if additional magnetic optical components are installed in series, since they do not have definite spin direction along the local magnetic field.

The gain $R(\lambda)$ measured at $(x, y) = (0, 0)$ clearly showed a broad peak at $\lambda \simeq 14.4$ Å as shown in Fig. 5. The focusing condition $\lambda = 14.4$ Å for 2000 mm sextupole field corresponds to $\omega = 432$ rad s^{-1} and the sextupole strength of $C = 3.2 \times 10^4$ T m^{-2}, which is consistent with the measured strength of $C = (3.5 \pm 0.6) \times 10^4$ T m^{-2}. The maximum gain was improved from the gain of 30 reported in Ref. [16]. The TOF spectra for the detector displaced off the magnet axis are shown in Fig. 6 for the cases of $x = 1$ and 2 mm. The magnet gain decreases according to displacements. The gain went below unity for the case of $x = 2$ mm at the focusing condition as most neutrons are focused on the magnet axis and hence fewer neutrons are observed off axis.

We define the peak gain $\bar{R}$ which is defined as

$$\bar{R} = \frac{\int_{14\,\text{Å}}^{14.8\,\text{Å}} N(\lambda)\,\mathrm{d}\lambda}{\int_{14\,\text{Å}}^{14.8\,\text{Å}} N_0(\lambda)\,\mathrm{d}\lambda}. \tag{9}$$

The values of $\bar{R}$ obtained according to the displacements of the detector center off the magnet axis are shown in Fig. 7. $\bar{R} = 36.5 \pm 8.0$ was observed at $(x, y) = (0, 0)$ on the magnet axis.

4. Simulation and discussion

The neutron motion inside the sextupole magnet was numerically simulated to extract the magnetic focusing effect and to identify the limiting factor of the magnet gain. Incident neutrons were generated uniformly at the entrance slit, which is a 2 mm diameter circle on the xy-plane located at $z = 2750$ mm. The neutron momentum was chosen to obey the angular distribution of $1 + \sqrt{3}\cos\vartheta$, where ϑ is the angle between the z-axis and the neutron momentum vector [20]. The trajectory of

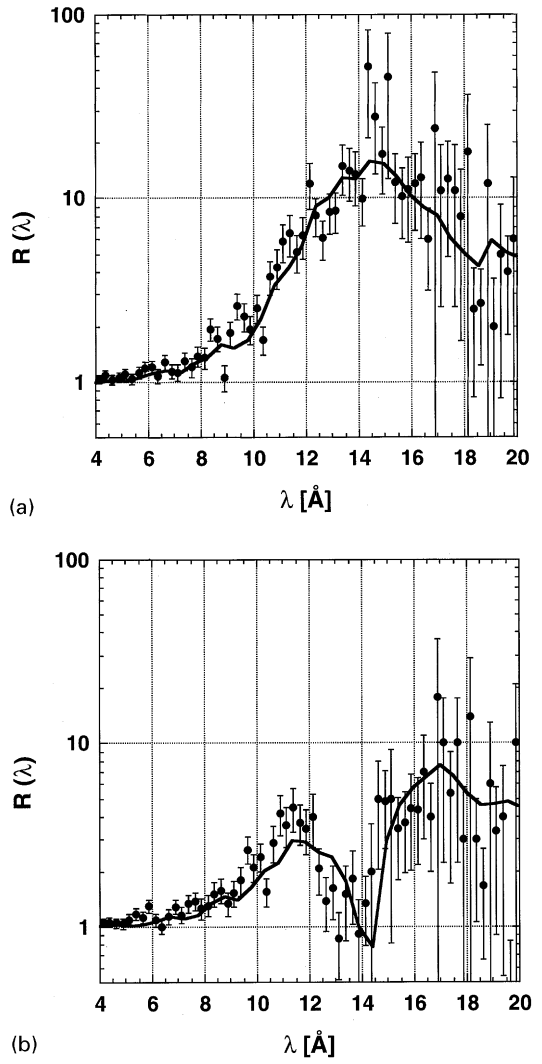

Fig. 6. Wavelength dependence of the magnet gain $R(\lambda)$ obtained off the magnet axis at (a) $(x, y) = (1\text{ mm}, 0)$ and (b) $(x, y) = (2\text{ mm}, 0)$. The solid lines show the calculated values of $R(\lambda)$ with $\Gamma_c = 0.057$.

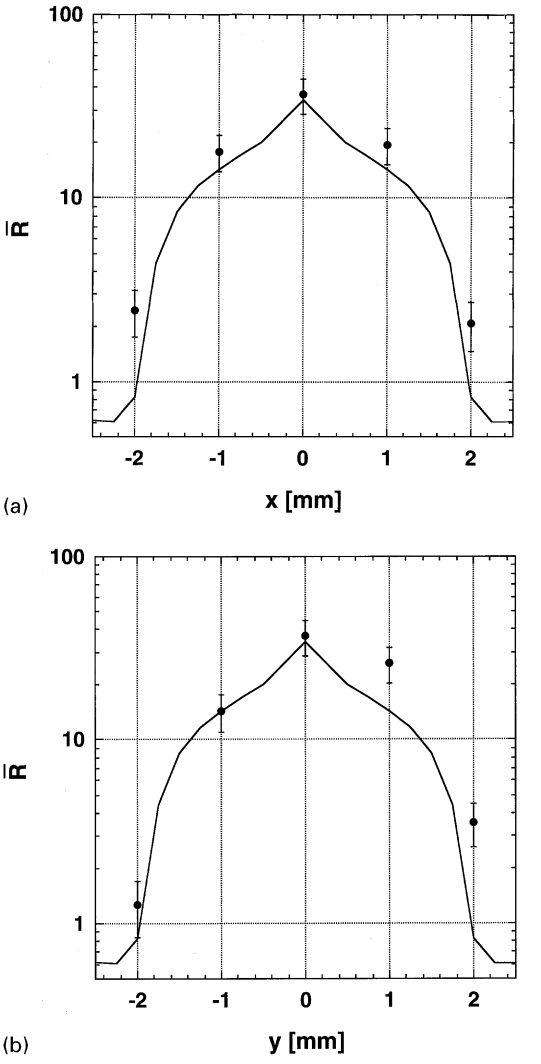

Fig. 7. Averaged gains at the peak ($\bar{R}$) are shown as a function of displacements from the magnet axis (a) on y-axis and (b) on x-axis. Asymmetry in (b) indicates the error in determination of the location of the magnet axis. The solid lines show the calculated values of $R(\lambda)$ with $\Gamma_c = 0.057$.

generated neutron was traced back onto $z = 0$ plane to calculate the starting position at $z = 0$ plane. If the starting position is out of the moderator area, another neutron was generated. The neutron intensity on the moderator surface was assumed to have the distribution of $\cos(\pi x/(w + 2\varepsilon))$ where $w = 150$ mm and $\varepsilon = 5$ mm, ignoring the y-dependence. The sextupole field was assumed to be effective only in the region of $2760 \leqslant z \leqslant 4760$ mm and no effect of fringing fields was taken into account. The trajectory was calculated analytically according to Eq. (6) and the neutron position at the plane of the second cadmium slit located at $z = 4780$ mm was calculated.

We assumed that there are two limiting factors of the magnet gain. One is the neutron reflection on

Table 2
Values of effective potential and surface roughness used in the simulation. The root mean square of surface roughness is shown in the table

	Effective potential (neV)	Roughness (r.m.s.) (μm)
Cadmium pipes	$44 - 18i$	0.1
Aluminum blocks	$54 - 10^{-3}i$	5.7

the inner surfaces of the magnet aperture. Reflected neutrons contribute to $N_0(\lambda)$ and decrease the value of $R(\lambda)$. The other is the non-adiabaticity around the magnet axis where the field is weak. The neutron spin polarization can be lost on the passage through non-adiabatic regions.

Neutron reflection and absorption was calculated on material surfaces in the magnet aperture. The reflectivities of cadmium and aluminum surfaces were evaluated according to the theoretical value of the effective potential and with the measured roughness as listed in Table 2. The reflectivity of NEOMAX48 surface was measured as shown in Fig. 8 using the reflectometer at JAERI [21]. Only the specular reflections were taken into account and the effect of the roughness was assumed to contribute only to a decrease in reflectivity.

The non-adiabaticity around the magnet axis was approximated by introducing a critical value of Γ in the following way. We introduced an adjustable parameter Γ_c and assumed that the neutron-spin polarization conserves completely in the region $\Gamma > \Gamma_c$ and it is completely lost once $\Gamma < \Gamma_c$ is satisfied on neutron trajectory, and travels without any effect of magnetic field until it exits from the region of $\Gamma < \Gamma_c$. The neutron spin is re-quantized upon exiting the region of $\Gamma < \Gamma_c$. In the cylindrical coordinate (ρ, ϕ), the Eq. (3) can be written as

$$\rho'' + \rho - \frac{\Lambda^2}{\rho^3} = 0 \tag{10}$$

$$\Lambda' = 0 \tag{11}$$

where $\Lambda = \rho^2\phi'$ and the primes represent the differentiation by θ. The solution is given as

$$\rho = \rho_0\sqrt{a + (1-a)\cos 2\theta + (\rho'_0/\rho_0)\sin 2\theta} \tag{12}$$

where $2a = 1 + (\rho'_0/\rho_0)^2 + (\Lambda/\rho_0^2)^2$. The normalized angular momentum Λ is conserved and the angular velocity increases as the neutron approaches the beam axis. The angular velocity of magnetic field direction in the neutron rest frame is $\omega_B = 2\dot{\phi} = 2\omega\Lambda/\rho^2$ and the Larmor frequency is given as $\omega_L = \gamma\rho^2 C/2$. The adiabatic condition $\Gamma \geqslant \Gamma_c$ gives

$$\rho \geqslant \rho_c = \left(\frac{4\alpha\Lambda\Gamma_c}{\gamma\omega}\right)^{1/4}. \tag{13}$$

We calculated the value of ρ_c for each neutron and checked if the trajectory goes into the region $\rho < \rho_c$.

For obtaining a crude estimation of Γ_c, we consider a classical magnetic dipole in a magnetic field rotating with a constant angular velocity ω_B. We put

$$\boldsymbol{\sigma}(\theta_B = 0) = \begin{pmatrix} 0 \\ 0 \\ 1 \end{pmatrix} \tag{14}$$

$$\boldsymbol{B}(\theta_B) = B\begin{pmatrix} 0 \\ -\sin\theta_B \\ \cos\theta_B \end{pmatrix} \tag{15}$$

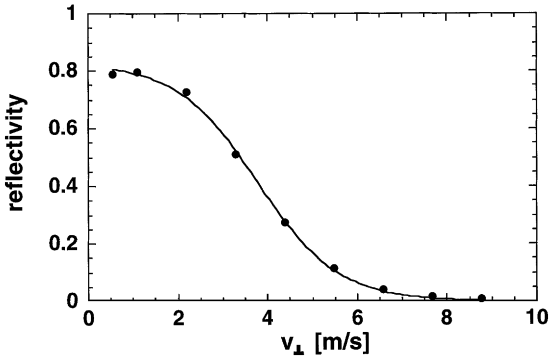

Fig. 8. Reflectivity of NEOMAX48 surface measured as a function of $v_\perp$, which is the neutron velocity component normal to the surface.

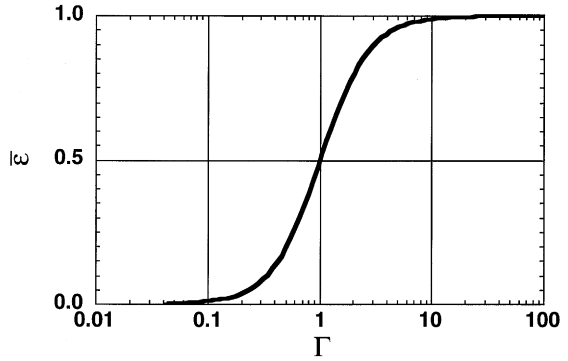

Fig. 9. Calculated values of $\bar{\varepsilon}$ as a function of Γ for the case that the ω_B is independent of time.

where $\theta_B = \omega_B t$. Eq. (2) can be written as

$$\frac{d\boldsymbol{\sigma}}{d\theta_B} = \Gamma \begin{pmatrix} 0 & \cos\theta_B & \sin\theta_B \\ -\cos\theta_B & 0 & 0 \\ -\sin\theta_B & 0 & 0 \end{pmatrix} \boldsymbol{\sigma} \tag{16}$$

where $\Gamma = \omega_L/\omega_B$. The component of neutron spin along the magnetic field direction is given as

$$\varepsilon(\theta_B) = \boldsymbol{\sigma}(\theta_B) \cdot \hat{\boldsymbol{B}}(\theta_B). \tag{17}$$

We define the time average of $\varepsilon(\theta_B)$ as

$$\bar{\varepsilon} = \lim_{\theta_B \to \infty} \frac{1}{\theta_B} \int_0^{\theta_B} \varepsilon(\theta)\, d\theta \tag{18}$$

where the value of $\bar{\varepsilon}$ is shown in Fig. 9. $\bar{\varepsilon}$ is the fraction of neutron polarization following the direction of magnetic field and gives a crude estimation of the neutron polarization remaining after traveling in the magnetic field for a long time. In actual cases, the remained neutron polarization is more complicated because each neutron experiences a different field according to its flight path and the magnetic field rotation is variable. Therefore, the parameter Γ_c should be chosen to be much less than unity as the neutron polarization is assumed immediately and completely lost at $\Gamma = \Gamma_c$. The parameter Γ_c was treated as the only free parameter to fit the measured TOF spectra. The peak gain $\bar{R}$ was calculated as a function of Γ_c as shown in Fig. 10. The best value of $\Gamma_c = 0.057$ was obtained to reproduce the peak gain of $\bar{R} = 35$ on the magnet axis. TOF spectra of $R(\lambda)$ with the value of

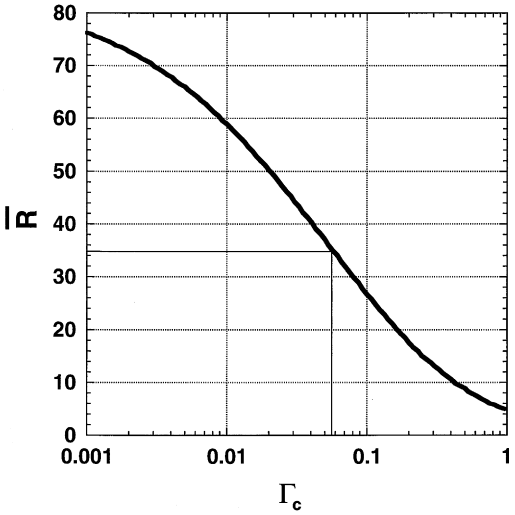

Fig. 10. Calculated values of $\bar{R}$ as a function of Γ_c.

$\Gamma_c = 0.057$ are shown in Figs. 5 and 6. The best fit value of $\Gamma_c = 0.057$ is naturally smaller than unity.

In the current experimental configuration, the peak gain $\bar{R}$ is limited by the reflection on the inner surface of the magnet aperture. In the case that the inner surface is completely black or the aperture is sufficiently large, the neutron gain is increased further. Under the condition of $C = 3.2 \times 10^4$ T m^{-2} which implies $\omega = 432$ rad s^{-1}, we calculated the value of peak gain $\bar{R}$ as a function of the aperture as shown in Fig. 11. The peak gain saturates with the value of $\bar{R} = 800$ with the diameter of the aperture at 30 mm. The maximum value of $\bar{R}$ depends on the moderator size, the configuration of the beam line and the sextupole strength. In the case of an aperture diameter of 30 mm, the magnitude of the magnetic field is $|\boldsymbol{B}| = 3.8$ T on the aperture boundary, which can be reasonably realized.

The non-adiabaticity is also limiting the gain. For greater improvement in the gain, the non-adiabaticity can be removed by applying an additional solenoid field along the beam axis as

$$\boldsymbol{B} = \frac{1}{2} \begin{pmatrix} C(y^2 - x^2) \\ 2Cxy \\ 2B_s \end{pmatrix} \tag{19}$$

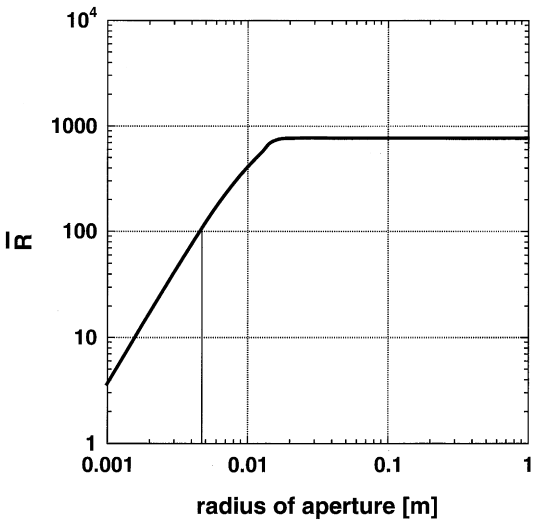

Fig. 11. Calculated values of $\bar{R}$ as a function of the aperture of sextupole magnetic field.

where $B_s \geqslant C\rho_c^2/2$. In the present experimental arrangement, the beam size is 2 mm in diameter. We take the maximum value of the velocity component perpendicular to the beam axis as $v_c = (v_{x,y})_{max} = 5$ m/s, which corresponds to the effective potential of the nickel surface of the neutron guide. We estimate the average value of Λ assuming the beam is uniformly distributed in the circle with the radius ρ_0 on xy-plane and in the square of $|\xi| \leqslant v_c/\omega$ and $|\eta| \leqslant v_c/\omega$ on the $\xi\eta$-plane as

$$\overline{\Lambda^2} = \frac{\int_0^{\rho_0}\rho\,d\rho\int_0^{2\pi}d\phi\int_{-v_c/\omega}^{v_c/\omega}d\xi\int_{-v_c/\omega}^{v_c/\omega}d\eta\Lambda^2}{\int_0^{\rho_0}\rho\,d\rho\int_0^{2\pi}d\phi\int_{-v_c/\omega}^{v_c/\omega}d\xi\int_{-v_c/\omega}^{v_c/\omega}d\eta} = \frac{1}{6}\left(\frac{\rho_0 v_c}{\omega}\right)^2 \sim 2\times10^{-11}\ \mathrm{m}^4. \quad (20)$$

If we take $\Gamma_c = 0.057$ and substitute Λ in Eq. (13) with $(\overline{\Lambda^2})^{1/2}$, we obtain $2\rho_c = 3\times10^{-4}$ m. This value is sufficiently small compared with the beam aperture. The small non-adiabatic region can be removed by applying a solenoid field along the magnet axis with the strength of $B_s \geqslant 5\times10^{-4}$ T.

The focusing sextupole field transports all neutrons inside the magnet aperture without beam loss. This feature is ideal for neutron transportation to distant spectrometers.

The magnetic neutron optics can be applied for the suppression of the beam divergence by applying the transformation M_A as schematically shown in Fig. 12. In the first sextupole field, the incident beam is rotated on the $x\xi$-plane by the angle θ_1, and is transformed by $M_0(\theta_2)$ in the intervening flat field. θ_1 and θ_2 are adjusted so that the transformed given straight line becomes parallel to the $(-1, 1)$ direction on the $x\xi$-plane;

$$\tan\theta_1 + \theta_2 + 1 = 0. \quad (21)$$

The neutron polarization along the local field in the sextupole field can be converted to a one-directional polarization by adiabatically connecting the sextupole field to a flat field. The sign of neutron polarization relative to the magnetic field is reversed on transmission through a non-adiabatic region. The second flat field is connected to another sextupole field adiabatically. Neutrons are transformed by M_A in the second sextupole field because the sign of polarization is inverted relative to the magnetic field. The second sextupole field compresses the beam by a factor of $\exp(-\theta_3)$ along $(-1, 1)$ direction. The converging beam is defocused and the beam divergence is suppressed on transmission through the second sextupole field. Consequently, a thin and small-divergence beam is obtained at the exit of the second sextupole by adjusting the length of the second sextupole field. In addition, a polarized neutron beam can be obtained by adiabatically transporting neutron polarization along the local magnetic field into a flat field.

In actual experiments, any neutron beam has a finite area on the $x\xi$-plane. The magnetic control of the neutron beam does not change the area on the $x\xi$-plane, while the point neutron source occupies null area. It should be noted that it is impossible to compress both the spatial beam size and beam divergence without losing any part of the incident beam, as the magnetic control does not change the area on the $x\xi$-plane.

The magnetic optics can be applied for a direct measurement of neutron momentum. A magnetic lens installed between a sample and a detector selectively focuses the scattered neutrons according to their wavelengths. A quadrupole magnetic field can function as a magnetic neutron prism since the

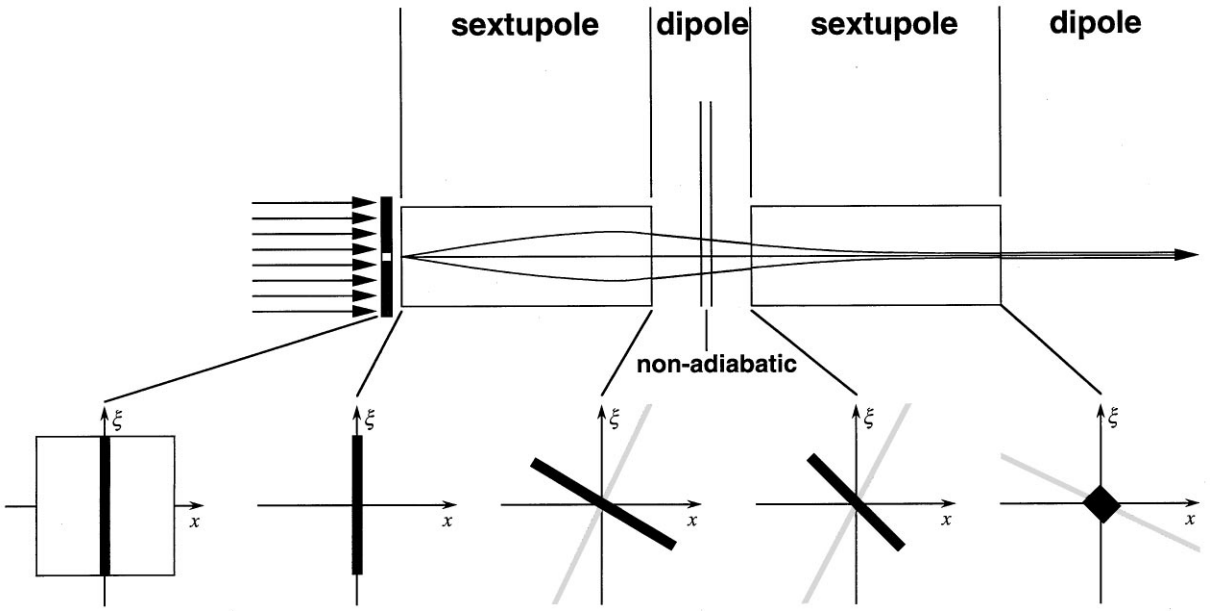

Fig. 12. Schematic illustration of the method to suppress both the spatial and velocity sizes in $x\xi$-plane.

neutron beam is dispersed according to the neutron wavelength. Therefore, the neutron momentum is directly measured using a position-sensitive neutron detector.

Higher multipole fields cause non-linear rotation, expansion and compression on the $x\xi$-plane, which introduce more variety of neutron beam control. Hybrid optics among magnetic optics, compound refractive optics and reflective optics have a potential in realizing more flexible beam control techniques.

5. Summary

The magnetic focus effects on cold neutron beams were studied by measuring the neutron intensity as a function of neutron wavelength upon transmission through a permanent sextupole magnet. The intensity gain of $\bar{R} = 35$ was observed at $\lambda = 14.4$ Å. The spatial distribution of intensity gain was also measured as a function of neutron wavelength. The measured results were successfully simulated by taking into account the neutron reflection on the inner surface of magnet aperture. It was also shown that the value of magnetic field gradient used in our experiment has the potential to achieve an intensity gain of $\bar{R} = 800$ if the magnet aperture is larger than 30 mm.

Acknowledgements

The authors are grateful to staff members of Development of Research Fundamentals Technology of The Institute of Physical and Chemical Research (RIKEN) for the construction of the sextupole permanent magnets. They acknowledge Mr. Iwasa for his support and the construction of experimental apparatus for the neutron beam experiments. They also thank Drs. M. Furusaka, Y. Kawabata and K. Soyama for their valuable suggestions and discussions.

References

[1] M.A. Kumakov, V.A. Sharov, Nature 357 (1992) 390.
[2] P.S. Farago, Nucl. Instr. and Meth. 30 (1964) 271.
[3] H.M. Brash et al., Proc. Roy. Soc. Edingburgh A 68 (part. 2) (1969) 158.

[4] G.I. Terekhov, Pis'ma Zh. Tekh. Fiz. 3 (1977) 1275 [Sov. Tech. Phys. Lett. 3 (1977) 526].
[5] J.H. Coupland, R.V. Stovold, Sixth International Conference on Magnet Technology, Bratislava, Czechoslovakia, 29 Aug.–2 Sep. 1977, p. 558.
[6] W.G. Williams, Polarized Neutrons, Clearendon Press, Oxford, 1988.
[7] Z.J. Yang, D.J.W. Geldart, R.A. Dunlap, Phil. Mag. B 68 (1993) 713.
[8] R. Golub, P. Carter, Nucl. Instr. and Meth. 91 (1971) 205.
[9] T.J.L. Jones, W.G. Williams, J. Phys. E 13 (1980) 227.
[10] M. Utsuro, J. Phys. Colloq. 45 (1984) C-3269.
[11] J. Summhammer, L. Niel, H. Rauch, Z. Phys.: Condens. Matter 62 (1986) 269.
[12] I.M. Matora, Yad. Fiz. 16 (1972) 624 [Sov. J. Nucl. Phys. 16 (1973) 349].
[13] K.-J. Kügler, W. Paul, U. Trinks, Phys. Lett. 72 B (1978) 422.
[14] K.-J. Kügler, K. Moritz, W. Paul, U. Trinks, Nucl. Instr. and Meth. A 228 (1985) 240.
[15] F. Anton et al., Nucl. Instr. and Meth. A 284 (1989) 101.
[16] H.M. Shimizu et al., Physica B 241–243 (1998) 172.
[17] A. Steinhof, Nucl. Instr. and Meth. A 397 (1997) 371.
[18] M.R. Eskildsen et al., Nature 391 (1998) 563.
[19] Y. Kaneko, K. Tokuhara, N. Ishigaki, Vacuum 47 (1996) 907 and references therein.
[20] Y. Kiyanagi, N. Watanabe, H. Iwasa, Nucl. Instr. and Meth. A 312 (1992) 561.
[21] T. Ebisawa et al., Physica B 213–214 (1995) 901.